Energy Conversion and Management 356 (2026) 121326

Contents lists available at ScienceDirect

Energy Conversion and Management

journal homepage: www.elsevier.com/locate/enconman

Research paper

Strategies for improving premixed oxy-fuel combustion in spark-ignition engines

R. Raggi, J. Gomez-Soriano, J. Martín *, R. Novella

CMT – Clean Mobility & Thermofluids, Universitat Politècnica de València, Camino de Vera s/n, 46022 Valencia, Spain

ARTICLE INFO

Keywords:
Oxy-fuel combustion
Zero NO_x
CO_2 capture
Efficiency
Carbon capture
MIEC

ABSTRACT

Oxy-fuel combustion in internal combustion engines is a promising technology that eases Carbon Capture and Storage and allows near-zero NO_x powerplants. While some experimental and theoretical studies on oxy-fuel combustion engines are available in the literature, there is a lack of systematic research on dilution strategies or on the use of non-synthetic exhaust gas recirculation. This study uses a combination of 0D-1D and CFD modeling and experimental measurements to assess the use of oxygen dilution and real exhaust gas recirculation in a single-cylinder spark-ignition engine operation under oxy-fuel combustion conditions. A comparison between conventional and oxy-fuel combustion is first performed to highlight the differences between the two combustion modes. Later, taking into account the thermo-mechanical limitations and knocking restrictions, several strategies are analyzed to improve oxy-fuel combustion efficiency: exhaust gas recirculation ratio, compression ratio, and intake temperature. Results show that under oxy-fuel mode, operating at stoichiometric conditions with exhaust gas recirculation rates around 70%, reduces NO_x by more than 99%, and CO and uHC by up to 89% compared to conventional combustion with air. In terms of performance, an 8 pp reduction in gross indicated efficiency could be expected; however, since knocking propensity is reduced, the compression ratio can be increased to recover about 5 pp of the efficiency drop.

1. Introduction

Over the years, measures have been put in place to reduce emissions and improve the energy efficiency of internal combustion engines (ICEs) to address the negative impacts of global warming. The European Commission has proposed a policy with targets for 2030 that aims to reduce greenhouse gas (GHG) emissions by 40% and increase energy efficiency by 32.5% [1]. Although ICEs are used in many sectors, the road and maritime transportation sectors have received significant attention, as they account for 25% and 13% of GHGs in Europe, respectively [2]. As a result, policies and regulations focus on developing low or zero-emission propulsive systems [3] and new, environmentally friendly fuels (e.g. biofuels and e-fuels) for the transportation industry [4].

Furthermore, to counter the implications of poor air quality on public health, the European Environment Agency (EEA) is responsible for the data acquisition of air pollutants submitted by the Convention on Long-Range Transboundary Air Pollution along the European Union [5]. Results revealed that road transport accounts for 28.1% of nitrogen oxide (NO_x) emissions, while the maritime sector accounts for 19.4%. In addition, CO emissions indicate that road transportation accounts for 18.0%. In this case, the maritime sector represents less than 1% of the impact. Carbon oxides (CO, CO_2) are caused by the oxidation of hydrocarbons during the combustion process, which are the main components of the fossil fuels used in ICEs. Moreover, NO_x is produced by the presence of nitrogen in the air. The increase in temperature produced by the combustion process enables the oxidation of this nitrogen, promoting the formation of NO_x mainly due to the thermal mechanism.

One potential solution that has been proposed to address the emissions issue associated with internal combustion engines (ICEs) is oxy-fuel combustion (OFC) [6]. This unconventional combustion mode has attracted increasing attention in recent years [7], particularly in spark-ignition (SI) engines, as it enables the exploitation of mature engine technology while progressing towards low- [8] or zero-emission [9] power generation concepts. Several experimental [10] and numerical [11] studies have investigated OFC in SI engines operating under oxygen-enriched atmospheres. Serrano et al. [12] showed that using EGR instead of O_2 as a diluent under stoichiometric conditions (60%–70% EGR) offers the best balance between stability, efficiency, and engine integrity. They also found that oxy-fuel combustion reduces knocking, allowing spark optimization and higher compression ratios to mitigate fuel consumption penalties. Yu and Wu [13] conducted

* Corresponding author.
E-mail address: jaimardi@mot.upv.es (J. Martín).

https://doi.org/10.1016/j.enconman.2026.121326
Received 15 December 2025; Received in revised form 27 February 2026; Accepted 4 March 2026
Available online 11 March 2026

experimental and simulation studies using a single-cylinder research engine. Their work evaluated the effect of water injection near top dead center (TDC) at different dilution levels using dry exhaust gas recirculation (dry-EGR, composed solely of CO_2), reporting indicated efficiency improvements of up to 46%. Similarly, Li et al. [14] numerically examined the influence of water injection in a gasoline SI engine operating under dry-EGR dilution conditions, observing that OFC led to an increase in brake-specific fuel consumption (BSFC) compared to conventional air combustion for different injection strategies.

While these studies provide valuable insight into the potential of OFC, they are based on idealized dilution strategies and do not address one of the main technological challenges of this combustion mode: the production and on-board supply of oxygen. To overcome this limitation, Arnau et al. [15] proposed a novel OFC engine concept with in-situ oxygen production, integrating the propulsion system with a mixed ionic and electronic conducting (MIEC) membrane [16]. In this configuration, the recirculated exhaust gas inherently consists of a mixture of CO_2 and H_2O [17], hereafter referred to as real or humid exhaust gas recirculation (from now on referred to as EGR). Their numerical results showed that, under these conditions, the engine efficiency was lower than that of a conventional SI engine, highlighting the complex thermo-chemical effects introduced by water vapor in oxy-fuel environments.

Despite its practical relevance, the role of humid EGR in oxy-fuel SI engines remains largely unexplored. To the authors' knowledge, all available experimental studies on OFC in SI engines have been conducted using dry EGR or idealized diluents, neglecting the presence of water vapor that inevitably arises in real oxy-fuel systems with exhaust gas recirculation. However, accounting for humid EGR is essential to realistically assess in-cylinder conditions, combustion behavior, knock propensity, and performance limits in retrofitted or newly designed multi-cylinder oxy-fuel engines.

In this context, the present work aims to address this knowledge gap by experimentally investigating oxy-fuel operation in a spark-ignition engine using real (humid) EGR. Specifically, the study is guided by the following research questions: (i) how does the use of humid EGR, as opposed to dry dilution or pure oxygen control, influence in-cylinder temperatures and knock-limited operation in an oxy-fuel SI engine? (ii) What are the main performance and emissions trade-offs between conventional air combustion and oxy-fuel combustion when realistic EGR compositions are considered? (iii) To what extent can the performance of an oxy-fuel SI engine be improved through combined control of dilution strategy, compression ratio, and intake conditions? By addressing these questions, this work seeks to experimentally assess the operating range and performance potential of oxy-fuel SI engines under realistic conditions, contributing to the evaluation of this concept from a product-viability perspective.

This paper is structured as follows. The next section presents the experimental setup and the numerical tools employed, together with their respective validation. Section 3 describes the methodology adopted to analyze oxy-fuel combustion in ICEs. Section 4 presents and discusses the results, focusing on the identification of optimal dilution strategies while accounting for the thermo-mechanical limitations of the engine. In addition, an experimental-theoretical comparison between oxy-fuel and conventional combustion is carried out, and potential strategies for performance improvement are discussed. Finally, Section 5 summarizes the main conclusions and highlights the key contributions of this work.

2. Materials and methods

In this section, first, the test cell used to perform the experimental test will be described. Subsequently, the theoretical tools used in this research will be presented. Finally, the methodology followed to obtain the results of this work will be defined.

Table 1
Main engine specifications.

Number of cylinders	1
Port Injection system	Bosch EV 14
Ignition coil	Hella 5DA 006.623-951
Spark plug	Bosch ZR7SI332S
Number of strokes	4
Cylinder displacement	454.2 cc
Compression ratio	10.7:1
Cylinder diameter	82.0 mm
Stroke	86.0 mm
Connecting rod length	144.0 mm

2.1. Engine and test cell characteristics

Experiments were conducted on a 450 cc spark-ignition single-cylinder engine (SCE), whose main characteristics are provided in Table 1. The engine includes a four-valve pent-roof cylinder head, a conventional spark ignition system, and an exhaust gas recirculation (EGR) circuit. Even though the engine is equipped with port injection (PFI) and direct injection systems, only a commercial PFI injector will be used in this study to eliminate charge inhomogeneities as a source of uncertainty. Taken together, the use of the conventional combustion chamber design and standard injection and ignition hardware makes the engine configuration representative of a real application. Of course, deviations from a production engine include the use of pure oxygen as the oxidizer and the enhanced level of control inherent to the SCE configuration. Both aspects, however, are essential for achieving the specific objectives of the present research.

The engine was installed in a test cell that was instrumented as shown in Fig. 1. The test bench was modified to supply compressed O_2 and CO_2 from two tanks. The CO_2 tank was used to provide the necessary oxidant dilution to maintain engine integrity during start-up. The mass flow of oxygen supplied with the tank ($\dot{m}_{O_2}$) was controlled to reach the desired O_2 dilution, quantified by the λ parameter that is presented in Eq. (1). This parameter is a function of the mass flow of fuel ($\dot{m}_f$) and the stoichiometric oxygen to fuel ratio (F_s).

$$\lambda = \frac{\dot{m}_{O_2}/\dot{m}_{fuel}}{F_s} \tag{1}$$

Once steady-state operation was achieved, the external CO_2 supply was replaced with EGR. The system was designed to be flexible and able to switch between conventional combustion and OFC modes, using a valve downstream of the intake settling chamber, and the CO_2 and O_2 flow control valves. An external compressor was used for conventional combustion cases to boost the engine.

A knife-gate valve was installed downstream of the exhaust settling chamber in the exhaust line to control exhaust back pressure. A high-pressure EGR system supplied the required levels of cooled EGR; the rate of gas recirculated is calculated using Eq. (2). To prevent H_2O condensation in the EGR and intake pipes, which can affect the accuracy of CO_2 measurement and EGR rate determination, a heat exchanger was installed before the EGR settling chamber to carefully regulate the temperature of these lines when the engine is operating in OFC mode. Independent oil and cooling circuits were commissioned to control fluid conditions, as shown in the schematic of Fig. 1.

$$EGR = \frac{\dot{m}_{EGR}}{(\dot{m}_{O_2} + \dot{m}_{EGR})} \tag{2}$$

In-cylinder pressure was measured using a Kistler piezoelectric sensor, with an additional piezoresistive pressure sensor installed at the cylinder liner near bottom dead center for pressure signal pegging. Two piezoresistive sensors were mounted to measure intake and exhaust pressure. During the experimental tests, all engine fluid temperatures were monitored and controlled using K-type thermocouples. NO_x, CO, and uHC emissions were measured by a HORIBA MEXA-7100EGR gas

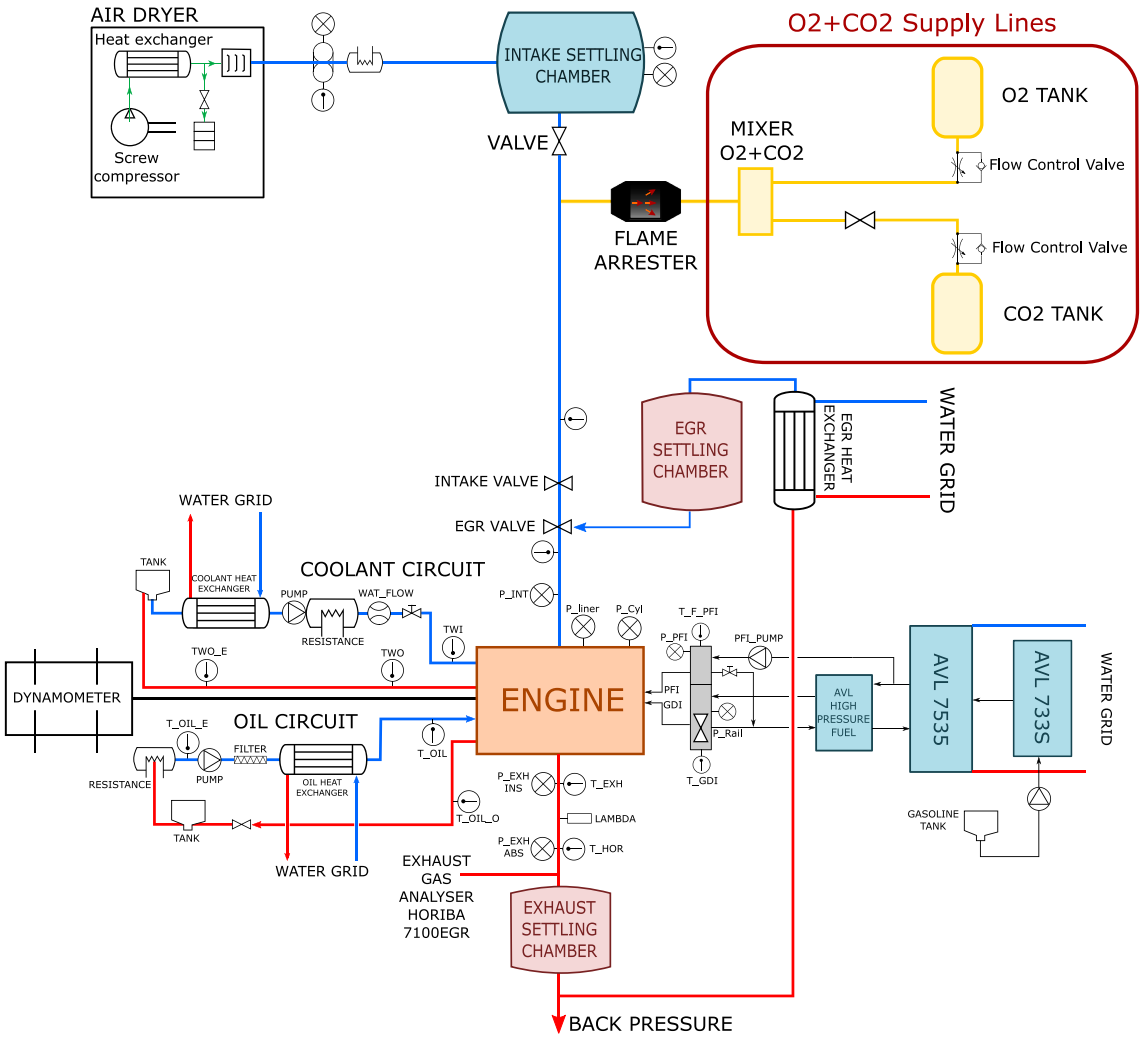

Fig. 1. Layout of the engine test cell.

Table 2
Summary and accuracy of the instrumentation used in the experiments.

Variable	Sensor	Accuracy
In-cylinder pressure	Piezoelectric sensor (Kistler 6054C)	0.2%
Temperature of all fluids	Thermocouples (K-type)	1.5 °C
Engine speed	Encoder	3 rpm
NO_x, CO and uHC concentration	Exhaust gas analyzer	3.0%
Intake, exhaust & pegging	Piezoresistive	0.35%
Torque	Torque meter	0.1 Nm
Fuel mass flow	Fuel mass flow meter (AVL 733S)	0.2%
Air mass flow	Air mass flow meter (Sensiflow D80)	2.0%

analyzer. This system was also used to measure CO_2 concentrations to calculate the EGR rate. However, a special device was necessary to dilute the gas sample to meet the gas analyzer's specification limit (up to 25% vol) when OFC is used, and N_2 is absent from the intake and exhaust flows. A summary of the instrumentation and its accuracy is provided in Table 2.

The global parameters related to the combustion process, i.e. the indicated mean effective pressure (IMEP), combustion phasing, maximum cylinder pressure, cycle-to-cycle variability (CoV_{IMEP}), and Heat Release Rate (HRR) were obtained from the in-cylinder pressure signal through the thermodynamic combustion analysis tool CALMEC [18].

2.2. Theoretical tools

Thermochemical modeling: Auto-ignition delay and flame temperature for various fuel-oxidizer mixtures and thermodynamic conditions were estimated through zero-dimensional (0D) chemistry calculations. Data was generated using a well-stirred reactor model at constant pressure to predict knocking tendency and maximum local temperatures. The ignition delay timing was defined as the time required to increase the temperature by 400 K from its initial temperature [19].

The chemical kinetic mechanism proposed by Liu et al. [20], based on a Primary Reference Fuel (PRF), was selected due to its good balance

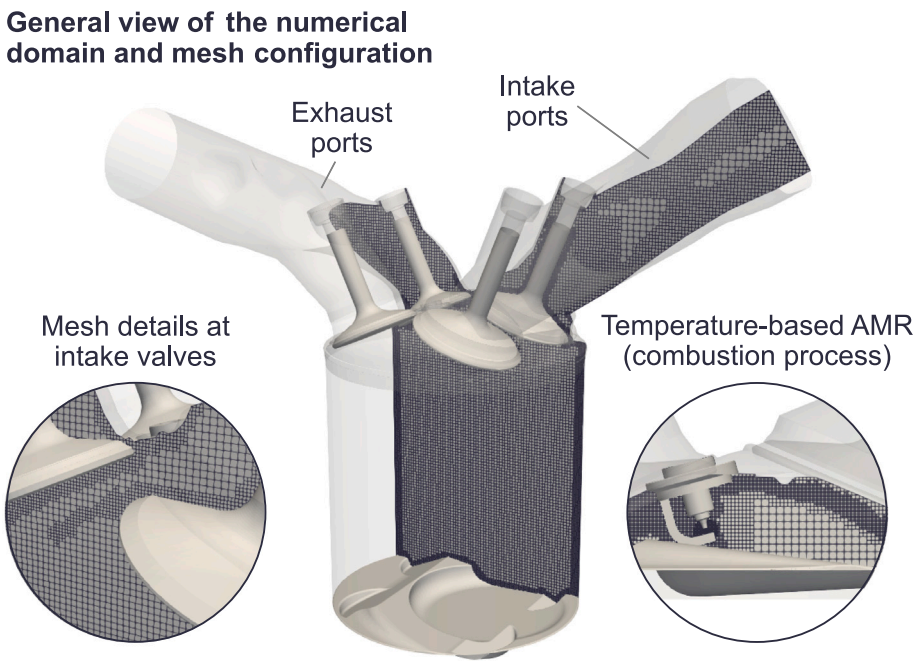

Fig. 2. Numerical domain and mesh characterization of the engine architecture.

between accuracy and computational demands. Benajes et al. [21] demonstrated the effectiveness of this mechanism under realistic and representative engine conditions, validating its results against experimental data reported by Fieweger et al. [22].

The laminar flame speed in a premixed oxidation reaction can be estimated by considering a freely propagating flame in a channel of fixed cross-sectional area at a given temperature, pressure, and mixture composition. Although this parameter is typically calculated using empirical correlations [23], they tend to under-predict laminar flame speeds at realistic engine conditions [21]. A 1D laminar flame speed solver was used to improve accuracy, and the chemical kinetic mechanism from Liu et al. [20] was selected due to its consistency with experiments conducted by Jerzembeck et al. [24] and Heimel et al. [25].

1D Fluid dynamic modeling: 0D-1D tools provide a good balance between accuracy and computation time [26]. To characterize the premixed OFC concept, in-cylinder pressure, temperature, gross indicated efficiency (GIE, calculated between −180 CAD and 180 CAD), and exhaust temperature were simulated using a 0D-1D tool for different EGR dilutions. The engine and test bench layout were implemented in the GT-SUITE code. These simulations reduce the need for experimental test campaigns while evaluating different engine strategies. In addition, a PID controller was implemented to optimize GIE by adjusting the start of combustion (SoC) while keeping the maximum in-cylinder pressure below 150 bar.

The model was calibrated using experimental data from the same engine operating in conventional SI mode at 3000 rpm and two different loads (4 and 11 bar of IMEP). In both cases, the in-cylinder conditions were simulated by imposing the experimental heat release rate obtained from the combustion diagnosis tool CALMEC. The validated results are summarized in a previous study [12], where the measured in-cylinder pressure and bulk temperature were compared to simulations, showing a good agreement at both 3000@4 and 3000@11 operating conditions (these conditions will be referred to as speed@IMEP).

CFD modeling: CFD simulations were conducted using CONVERGE v2.4 CFD software [27], a commercial code based on the finite volume method designed explicitly for ICE applications. The model represents the engine geometry, including the combustion chamber and intake/exhaust ports.

Table 3
Mesh configuration details.

Base size	4 mm
Intake/exhaust ports	2 mm
Chamber refinement	1 mm
Walls refinement	0.5 mm
AMR min. size	0.125 mm
Spark refinement	0.0625 mm
Number of cells	0.5–4 million

As shown in Fig. 2, a hexahedral grid strategy based on an orthogonal basis was used to mesh the entire computational domain with a base cell size of 4 mm. The mesh was refined to 2 mm at the intake and exhaust, and 1 mm in the cylinder. The cell resolution was increased (to 0.5 mm) near the cylinder walls, including the moving piston and valves. An Adaptive Mesh Refinement (AMR) algorithm was also employed to increase the grid resolution where spatial gradients in velocity and temperature are significant. This algorithm used a sub-grid criterion of 1 m/s and 2.5 K to decrease the cell size to a minimum of 0.125 mm. Finally, the grid resolution was further refined by reducing the mesh size up to 0.0625 mm at the spark gap electrodes to capture the initial flame kernel development. Full details about the grid definition are given in Table 3.

The turbulence was modeled using the unsteady Reynolds-averaged Navier–Stokes (URANS) framework, and the Re-Normalization Group variant of the k-ϵ model (RNG k-ϵ model [28]), that uses an eddy-viscosity-based two-equation approach. The gas-to-wall heat transfer was modeled by the model proposed by Angelberger [29], widely used in ICE applications [30].

Simulations were run using a second-order central difference scheme for spatial discretization and a first-order scheme for temporal discretization. The Pressure Implicit with Splitting of Operators (PISO) algorithm, as modified by [31], was used to couple the pressure and velocity fields. The ideal gas equation of state was considered to calculate the compressible flow properties.

The combustion process was modeled by the detailed chemistry solver proposed by Senecal et al. [32]. Besides, a multi-zone (MZ) approach was used to reduce computational time, with a 5 K temperature bin share [33]. Previous investigations [34] demonstrated that

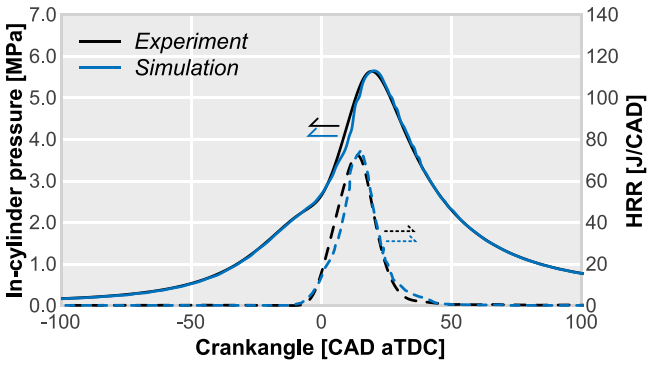

Fig. 3. Validation of CFD simulations at 3000 rpm and 11 bar IMEP. In-cylinder pressure signal and HRR trace are considered in the process.

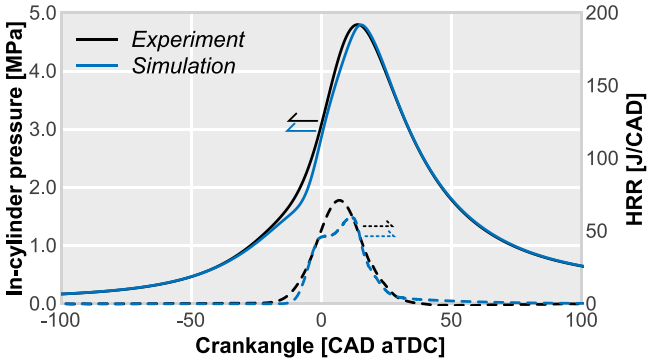

Fig. 4. Validation of the numerical method for OFC. The in-cylinder pressure signal and HRR trace obtained from CFD simulations at 3000 rpm, 11 bar of IMEP, $\lambda = 1$, and 70% of EGR are contrasted.

this approach is suitable for URANS-based gasoline combustion, even considering that it does not use an explicit turbulent combustion closure [35]. The chemical kinetic mechanism proposed by Liu et al. [20] was used for mimicking the thermochemical properties of the fuel. Energy deposition of 40 mJ was spatially and uniformly distributed in a sphere of 0.5 mm along an L-type profile [36] to simulate the ignition surface. This spark kernel was modeled by a volumetric source located between the spark plug electrodes.

The inflow and outflow boundary conditions at the ends of the intake/exhaust ports were defined by the instantaneous pressure signals measured during the engine tests. The surface wall temperatures were predicted by a lumped model [37].

The model was validated with the same experimental data used to tune the 0D-1D thermodynamic model. A comparison between experiments and CFD-simulated results at 3000@11 is shown in Fig. 3, where a reasonable prediction of the in-cylinder pressure and HRR signals was achieved.

As a final step, the numerical method's reliability is verified by comparison with OFC experiments conducted on the test bench. In Fig. 4, the variables simulated with the described 0D-1D-CFD method are compared to the measured ones at 3000@11 operating point applying a 70% EGR dilution with 850 mbar and 303 K of intake pressure and temperature, respectively. Although there are certain differences in the HRR peak, the results reasonably mimic the pressure evolution and accurately predict the start and the duration of the combustion process. Considering that none of the sub-models have been precisely adjusted for OFC, the results are promising, and the method can be used for performing further studies.

The numerical procedure was demonstrated to be a fast and effective way to obtain engine outputs when operating with OFC at maximum GIE conditions across different levels of EGR, thereby enabling analysis of engine performance and assessing the feasibility of the concept.

2.3. Methodology

In order to achieve the objectives of this work, the methodology depicted in Fig. 5 has been followed. First, 0D-1D thermochemical simulations have been performed at different EGR and λ rates to evaluate their impact on flame temperature, laminar flame speed, and auto-ignition delay, with the objective of assessing the best dilution strategy in OFC mode. These three parameters will set the main thermo-mechanical limitations that a spark-ignition engine must fulfill under OFC. Then, a validation procedure using experimental EGR sweeps will be carried out with $\lambda = 1$, the selected best strategy. In addition, the limits obtained from the previous thermochemical simulation analysis will be validated.

Secondly, experimental data from the single-cylinder engine were used to calibrate and validate the 1D fluid-dynamic model, ensuring accurate reproduction of the main operating variables (intake and exhaust pressures, temperatures, and gas flows), in-cylinder conditions, and overall engine performance. This was achieved by imposing experimentally derived heat release from conventional combustion tests and by refining air-path losses and heat transfer in the pipes and cylinder walls. At this stage, the 1D fluid-dynamic model is ready to be coupled with the CFD model as follows.

The coupling methodology (hereafter referred to as 1D-CFD) is detailed in a previous work and validated against experimental data [12]; in brief, the 1D model simulates the complete cycle and provides the instantaneous intake and exhaust manifold pressures as boundary conditions for the CFD calculations. The heat release from the CFD model is then fed back into the 1D model to calculate in-cylinder conditions and evaluate the performance of the oxy-fuel combustion concept in a short iterative process, repeated until convergence of the in-cylinder pressure calculated by the 1D model and heat release from CFD is achieved. It typically requires two to three iterations. This coupling strategy limits uncertainty propagation across modeling levels. Thus, experimental measurements from the engine are used to calibrate the 1D simulation, ensuring reliable boundary conditions for the CFD calculations, while the combustion process, the most sensitive and physically complex aspect of the OFC concept, is resolved using CFD and cross-validated against experimental pressure traces and heat release at representative OFC operating points, thereby strengthening the robustness of the combined framework.

Following, experimental and simulation results are used to compare oxy-fuel and conventional combustion by analyzing in-cylinder pressure data and assessing combustion characteristics, engine performance, and emissions to identify the main differences and their underlying causes.

In addition to the EGR effects experimentally evaluated, the investigation focuses on two other parameters that may improve the efficiency of OFC engines: the compression ratio (CR) and intake temperature. They are finally evaluated using the combination of 1D fluid-dynamic and CFD simulations.

Table 4 shows the operating conditions used in this research. They were chosen to balance the expected outcomes with the number of tests and simulations. These operating conditions are characterized by a constant engine speed (3000 rpm) and different engine loads (around 4, 11, and 21 bar of IMEP). The most relevant operation variables in the three experimental conditions are also detailed in Table 4. Note that low and medium engine loads (Points 1 and 2, respectively) were measured in the test bench and modeled, while the high load operating point (Point 3) was only simulated.

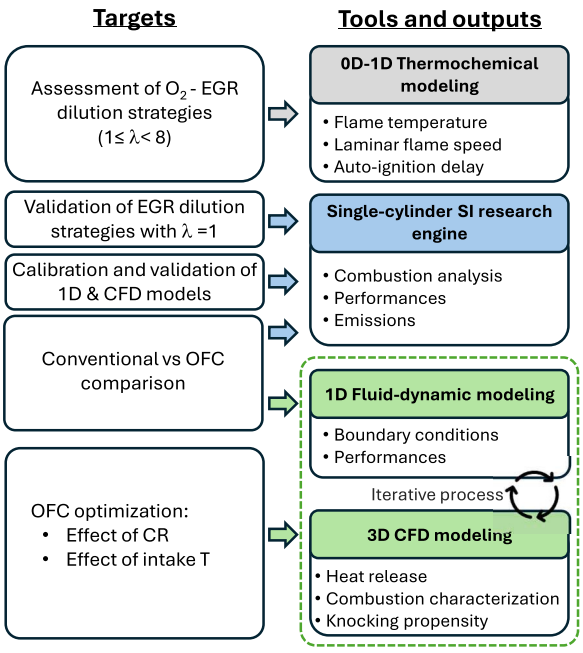

Fig. 5. Methodology flowchart.

Table 4
Operating parameters of the reference operating conditions using conventional SI combustion at stoichiometric conditions.

Operating point	Point 1	Point 2	Point 3[a]
Engine speed [rpm]	3000	3000	3000
IMEP [bar]	3.7	10.7	21.4
Injected fuel quantity [mg/cc]	10.6	33.15	66.3
Spark timing [CAD]	−16.6	−19	−19
Coolant temperature [°C]	80	85	85
Oil temperature [°C]	90	92	92
Intake pressure [bar]	0.41	0.98	1.37
Intake temperature [°C]	31	33	38

[a] Only evaluated by simulations.

3. Results and discussion

In this section, results, along with a discussion of the different outcomes, will be presented. First, the dilution rates will be assessed to later compare conventional and oxy-fuel combustion. Then, several strategies will be explored to evaluate each of their potential to improve efficiency.

3.1. Assessment of dilution rates

As a first stage, the impact of different dilution strategies on the most relevant combustion parameters was studied. In addition, this will provide information about the dilution ranges for suitable OFC. In Fig. 6, the flame temperature, the laminar flame speed, and the auto-ignition delay (AID) are depicted as a function of λ and EGR rate at Point 2 (3000 rpm and IMEP close to 11 bar) and in Table 5. If the engine operates without EGR, it will require λ values below 5 to keep the flame temperature below the 3000 K threshold and below 6.5 to achieve a minimum laminar flame speed that guarantees combustion stability. Alternatively, if only EGR is used to dilute the intake mixture, EGR rates must be higher than 61% to account for the aforementioned temperature limitations and lower than 75% to ensure combustion stability. Combined dilution strategies with both λ and EGR can also be used; thus, as λ increases from 1 to 5, the EGR rate should decrease from 61% to 0% to keep the adiabatic temperature limit below 3000 K.

Table 5
Limits defined for assessing the dilution strategies.

Parameter	Value
Flame temperature [k]	3000
Laminar flame speed [m/s]	0.5
Auto-ignition delay [ms]	3

In the same way, while λ increases from 1 to 6.5, EGR must decrease from 75% down to 0% to keep a stable combustion process.

After defining the dilution range in which the concept could be used, a technological evaluation was conducted to determine the best strategy. On the one hand, the in-cylinder mixture can be diluted, increasing the λ, which will require a higher in-situ O_2 production or, in any case, a higher consumption from the O_2 source. As discussed in [38], this would lead to an oxygen transport membrane (OTM) requiring more energy flow (thermal and/or electrical) to separate the O_2 from the N_2. In addition, if this strategy is followed, the exhaust gases will be composed not only of CO_2 and H_2O, but also of an important amount of O_2. The most suitable way to capture CO_2 is the compression and cooling down of the exhaust flow until reaching CO_2 conditions close to critical ones (about 75 bars and 30 °C); in slightly more conservative conditions (80 bars and 20 °C) the liquid–vapor equilibrium of CO_2 and O_2 mixture leads to an O_2 mass fraction of about 5% in the liquefied mixture captured when operating with λ around 1.1 and hence captured CO_2 quality is worsened. Furthermore, AID values indicate that knock might occur when EGR is below 40% and λ is above 3; thus, this region must be avoided. On the other hand, dilution via EGR is a widely used technique in conventional engines, as Desantes et al. [39] applied to different layouts in a multi-cylinder OFC engine. Additionally, it should be noted that this strategy is more efficient at controlling in-cylinder temperature than O_2 dilution, because the specific heat of EGR (CO_2 and water) is higher than that of O_2. Finally, it must be considered that operating with an excess of O_2 entails relevant trade-offs in terms of efficiency and emissions. From an efficiency perspective, experimental results show that increasing the equivalence ratio from λ= 1 to λ= 1.2 increases gross indicated efficiency by approximately 2 percentage points; however, this benefit is accompanied by a significant increase in NO_x production, which is almost completely suppressed under stoichiometric conditions.[1] Under lean operation, the increase in NO_x is an additional limiting factor, as the use of a three-way catalyst is no longer feasible. In contrast, stoichiometric operation enables the use of an oxidation catalyst (to control CO and uHC) or a three-way catalyst (if NO_x traces must be completely eliminated); in both cases, it is a mature, robust, and relatively low-cost aftertreatment solution. As a result, while lean operation may offer modest efficiency gains, the associated emissions penalty and aftertreatment constraints further support the choice of stoichiometric operation. All these reasons led to selecting, as a strategy in premixed OFC, the operation with $\lambda \approx 1$ and recirculated exhaust gases. It is important to emphasize that this conclusion may not apply to diffusion combustion, where the controlling phenomena, main issues, and limitations can differ.

The preceding analysis does not consider the 3D complexity taking place in the combustion chamber; in a previous work [12], the 1D-CFD approach used in Section 3.3 was used to refine the maximum EGR dilution rate, in stoichiometric conditions, that guarantees the combustion stability; a value of 73% was found. With the EGR range [61%-73%] from simulations in mind, this work first conducted an experimental campaign to validate this operating range at 3000@11.

[1] As discussed later, NO_x is not completely suppressed under OFC conditions due to trace amounts of nitrogen entering the combustion chamber from various sources still lead to measurable NO_x emissions.

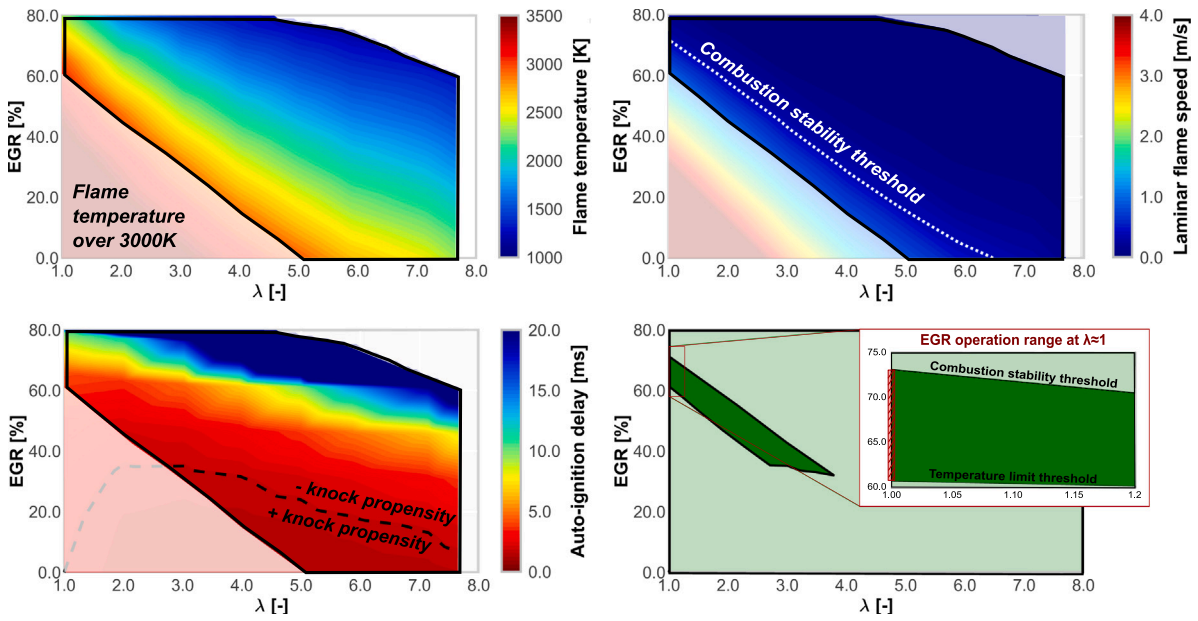

Fig. 6. Analysis of chemical simulations at 3000 rpm and 11 bar IMEP.

Although the engine performance is later discussed in detail in Section 3.3.1, at this point, it is worth highlighting two main findings. On the one hand, 67% was the lowest EGR rate that was able to be achieved experimentally; these lowest dilution conditions produced an exhaust temperature of 1200 K (about 930 °C) that was over the specifications limit provided by the engine manufacturer, and thus no further EGR reduction was measured to avoid compromising the engine and instrumentation safety. It is expected that, without the aforementioned thermal limitation, it would be possible to achieve the 61% dilution rate predicted by the 0D-1D combustion model. No knocking issues were found, confirming that, according to Fig. 6 (bottom), these conditions are far from the dilution region where it is likely to happen. In any case, as later discussed, a lower EGR rate will not be of interest from a thermal efficiency perspective.

On the other hand, 73% was the highest EGR rate experimentally achieved, and thus the predicted value agrees with the measurements. In this case, the limitation was the combustion stability due to the over-dilution. These results allow concluding that, in spite of its simplicity, 0D-1D simulation is valid to perform this type of estimation, and both experimental and simulation tools allow confirming the operation range of the premixed oxi-fuel combustion in the EGR ranges of [61%-73%] at medium speed and load (3000@11) and $\lambda = 1$; this experimental-theoretical range is included, in red, at the top of Fig. 6. As discussed later, this range can vary depending on the compression ratio and engine load.

3.2. Conventional vs oxy-fuel combustion

After deciding to use the EGR dilution strategy (within a limited range) to control in-cylinder temperature, experimental tests allowed assessing differences between oxy-fuel and conventional combustion. Starting from the in-cylinder pressure signal and using the combustion analysis tool CALMEC [40], the evolution of the in-cylinder temperature, heat release (HR), and heat release rate (HRR) was obtained as a function of the crank angle. In this section, the main concepts to understand the difference between the two combustion modes will be presented; however, a more detailed analysis of this comparison can be found in [10].

The following analysis was performed at 3000@11 (Point 2), under stoichiometric conditions, and with an EGR rate of 70% for the OFC case. It is worth noting that this EGR value was used because, as discussed in [10], it provides the highest indicated efficiency while maintaining low cycle variability. For the conventional combustion case, no EGR was used. Additionally, among all cases with an OFC measured at a 70% EGR ratio, the case with a spark timing of −20 CAD was selected to maintain the same combustion phasing between the two combustion modes.

Due to the intrinsic differences in intake conditions and composition, the mass and thermodynamic conditions at inlet valve closing are different; however, to ensure comparable operation under both conditions, both fuel mass and combustion centering (CA50) were kept constant. The main issues analyzed are the following:

- As shown at the top of Fig. 7, during the compression stroke, the pressure is higher in the conventional combustion. Even though the pressure at the IVC is 180 mbar lower in OFC, a quick analysis shows that this value does not explain the differences at the start of combustion (SoC = −15 CAD). Thus, taking into account the 180 mbar difference at the IVC, a polytropic compression with a constant exponent of 1.34, as obtained from compression under conventional conditions, will result in a 2 bar variation at the SoC. As can be seen, the experimental evolution of the in-cylinder pressure shows a larger difference of about 7 bar at this point. OFC EGR gases are mainly composed of CO_2 and H_2O vapor; thus, its adiabatic expansion coefficient is expected to be reduced around 7% with respect to conventional SI (where the diluent is composed of N_2), as can be seen in Fig. 8. This gamma reduction leads to an increase in the pressure gap between the two combustion modes of around 50%. The aforementioned change in properties also has an analogous effect on the in-cylinder temperature under OFC (for the sake of rigour, it is lower because the exponent of the pressure ratio is less than 1 in the polytropic expression). It can be seen that even though the temperature at IVC is higher, it is almost the same at the SoC. This was targeted to partially compensate for differences in IVC conditions resulting from different intake and exhaust processes.
- During the combustion phase, slightly slower combustion is obtained with OFC, as shown at the top of Fig. 9. This effect, along with the mixture's higher specific heat, results in a lower maximum temperature when the engine operates with OFC.
- After combustion completion (beyond 35 CAD), a lower value of γ during the expansion phase produces an effect similar to

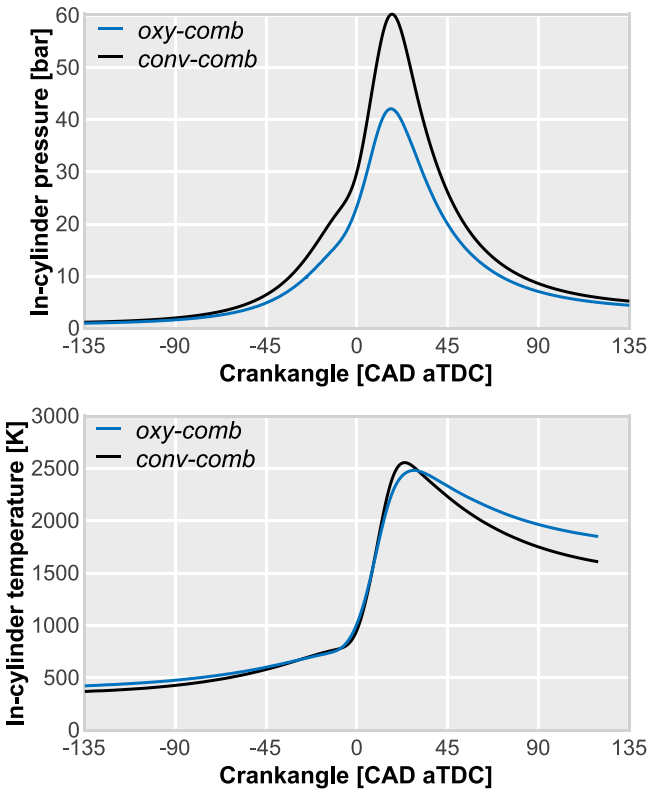

Fig. 7. Comparison of in-cylinder pressure signal (top) and in-cylinder temperature evolution (bottom) between OFC with 70% EGR dilution and conventional SI combustion concept at 3000@11 and $\lambda = 1$.

that observed during compression, namely a reduced temperature rate of change and, consequently, a final temperature at exhaust valve opening (EVO) approximately 300 K higher under OFC conditions than in conventional combustion. This change must be taken into account in both the engine design and the engine control restrictions: in the first case, to avoid exceeding the thermal limits of the engine components; in the second, because higher exhaust temperature is an advantage when O_2 production is performed with an OTM. Thus, it must be taken into account that the performance of this element is strongly dependent on the temperature, which shows an increase of 153 K in the OFC case (see Table 6). In addition, a reduction in the maximum pressure of almost 18 bar was observed due to differences in pressure at SoC and slower combustion during OFC.

- Both HRR and accumulated HR graphs show that, for a constant $CA50 = 11$ CAD, the combustion process is longer in OFC with a combustion duration ($CA90 - CA10$) of 25 CAD, in contrast with approximately 22 CAD in the conventional case. This trend can be explained by the lower laminar flame speed, estimated at about 0.6 m/s in OFC for $\lambda = 1$ and EGR=70%, whereas in the conventional case it exceeds 1 m/s. Moreover, this slower combustion leads to the previously commented reduction in the HRR peak by 10 J/CAD, as depicted at the top of Fig. 9.

Table 6 shows oxygen mass fraction (Y_{O_2}), the GIE, the temperature in the exhaust manifold, and the main emissions for both combustion concepts to initially highlight the benefits and drawbacks. As shown, both cases have a Y_{O_2} of approximately 23%; this was set to facilitate the comparison between the two combustion modes. In terms of efficiency, a loss of around 8.7 percentage points was measured; this will lead to a discussion in the next section of possible strategies to improve the performance. To determine the origin of this performance, the heat

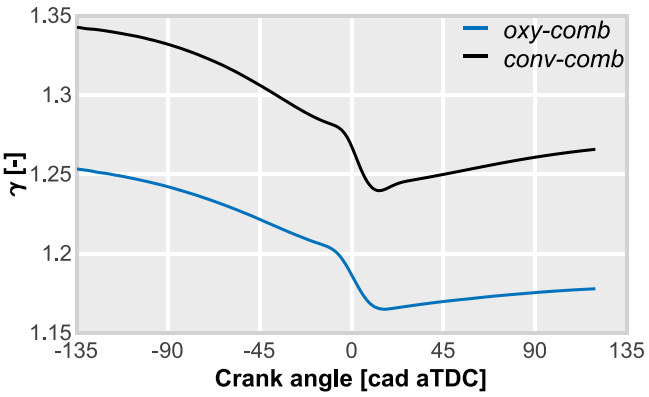

Fig. 8. Comparison of γ evolution between OFC with 70% EGR dilution and conventional SI combustion concept at 3000@11 and $\lambda = 1$.

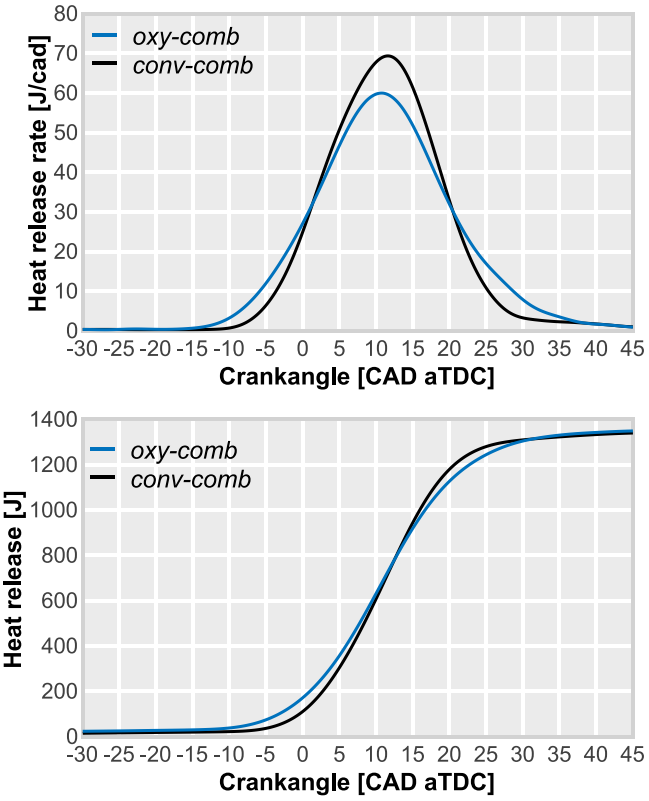

Fig. 9. Comparison of the evolution of the heat release rate (top) and cumulative heat release (bottom) between OFC with 70% EGR dilution and conventional SI combustion concept at 3000@11 and $\lambda = 1$.

transfer to the walls (piston, liner, and cylinder head) was first assessed. For both cases, the heat transfer (Q_w) was calculated using the Woschni empirical correlation. Results showed a 15% reduction in Q_w under OFC, which can be attributed to the lower in-cylinder pressure observed during this combustion mode. However, because the GIE is lower for the OFC cases, a higher Q_w would typically be expected; therefore, the penalty's root cause must be attributed to other parameters. Next, the difference in combustion duration (CA90-CA10) was analyzed. While the duration is 21.3 CAD under conventional combustion, it increases to 26.1 CAD in the OFC case. This represents a 22.5% elongation, which, according to estimations with an in-house 0D thermodynamic tool, results in a reduction in efficiency of approximately 1 percentage point. While this explains part of the efficiency loss, it is not the dominant

Table 6
Experimental performance and emissions comparison between an OFC and a conventional SI case for a constant CA50.

Parameters	OFC	Conventional SI
Y_{O_2} [%]	23.1	23.2
GIE [%]	29.8	38.5
Exhaust temperature [K]	1128	975
NO_x [g/kg$_{fuel}$]	0.03	65.32
CO [g/kg$_{fuel}$]	12.91	111.53
uHC [g/kg$_{fuel}$]	1.72	16.08

factor. Finally, the value of γ was examined, as it directly influences the theoretical thermal efficiency. Considering an Otto cycle and accounting for the 7% lower γ under OFC (as detailed in Section 3.2), this reduction in the ratio of specific heats is expected to decrease thermal efficiency by approximately 10 percentage points. Consequently, it can be concluded that the origin of the OFC efficiency penalty is primarily driven by the thermal properties of the oxy-fuel gas mixture.

Following the comparison between conventional and OFC, measurements indicate that NO_x emissions have been significantly reduced by 99.9%, thanks to the absence of N_2 under OFC operation. The remaining 0.03 g/kg$_{fuel}$ mainly originates from N_2 present in the fuel composition (0.15%) and lubricating oil, as well as from residual air ingress into the gas path. Such air ingress may occur through the crankcase ventilation system or minor sealing leakages, especially at low-to-mid loads where sub-atmospheric intake pressure is common. Although the resulting N_2 fraction is small, it can still lead to measurable NO_x formation. Regarding CO and uHC, both were abated by 88.4% and 89.3%, respectively. Despite similar O_2 fractions, the lower CO and uHC emissions observed under OFC conditions can be mainly attributed to the higher temperatures maintained during the late expansion and at exhaust conditions. These elevated temperatures extend the effective oxidation period after the main combustion event, promoting additional in-cylinder and post-combustion oxidation of CO and uHC before chemical reactions freeze. The higher water vapor content in OFC may also contribute to faster oxidation kinetics (by enhancing OH concentration), though this effect is secondary to the dominant thermal effect. These results suggest that this unconventional combustion mode is a promising approach for addressing the three emissions considered.

In addition to the experimental measurements, CFD simulations were carried out to assess the differences in the combustion process of conventional and OFC (with the same dilution conditions used in the experimental comparison). A qualitative analysis was conducted to examine the morphology of the flame front. Fig. 10 shows the in-cylinder flame evolution at different phases of the combustion process, considering both combustion modes. As shown, no significant differences in flame shape or progression are evident. Only a small difference appears in the initial combustion process (CA10-CA25) in the top view. It appears that the flame front propagates more rapidly towards the exhaust valves in conventional combustion. However, these differences become lower once the combustion process is established (CA50-CA75).

Furthermore, the premixed flame regime at different combustion timings was estimated to compare the two combustion concepts and to validate the combustion modeling approach used in the CFD simulations. To this end, turbulent properties (u' and l_t), laminar flame thickness (l_f), and laminar flame speed (s_L) are computed from the CFD results and included in the Borghi-Peters diagram of Fig. 11. Results indicate that OFC is expected to be in the *corrugated flamelets* regime as in the case of conventional SI combustion. Taking into account that both l_t and u' are similar between OFC and conventional combustion, the differences shown in the graph can be attributed to a lower s_L and l_f. This causes a shift from left to right and from bottom to top in the diagram, but always staying within the zone of *corrugated flamelets*. The similarity in flame morphology shown above stems from the fact that both concepts lie in the same region of the Borghi-Peters diagram. Therefore, the flame dynamics is still dominated by the corrugation of the front and hence, the burning velocity scales directly with the Reynolds number.

Consequently, any combustion model based on the *flamelet* hypothesis will be valid for OFC. In this context, widely used turbulent combustion models such as the G-equation, the Flamelet Generated Manifold (FGM), and the Extended Coherent Flame Model (ECFM) rely on this assumption. These models are standard in both CFD engine simulations and lower-order modeling frameworks (e.g., 0D and 1D approaches) due to their robustness and computational efficiency in describing premixed combustion regimes.

After establishing the validity of the *flamelet* assumption for OFC operation, it is also important to qualitatively assess how the combustion regime and flame structure might evolve under the different control strategies employed in this study. In particular, variations in EGR, CR, and intake temperature (T_{intake}) can significantly affect the turbulence–chemistry interaction, thereby influencing model applicability and combustion stability. The following discussion provides a qualitative analysis of these effects.

Increasing the EGR dilution reduces the laminar flame speed (s_L) and increases the flame thickness (l_f) [41]. This corresponds to a diagonal shift in the Borghi diagram, from the lower-right towards the upper-left, i.e., towards higher Karlovitz numbers and the region of *Thickened Wrinkled Flames*. This movement is the most critical, since small variations in EGR can lead to combustion regimes far from the *flamelet* assumption. In extreme cases, this shift can even cross the Damköhler number boundary of 1, entering the *Thickened Flame* region. However, the EGR values used in this investigation induce changes that remain moderate. Thus, although the conditions may enter the *Thickened Flame* region, the combustion models considered are deliberately adapted (e.g., by Peters [42] in the case of the G-Equation) to operate reliably under these conditions.

Increasing the compression ratio leads to higher in-cylinder pressures, which reduces s_L and decreases l_f [12]. This trend is similar to the shift observed when switching from conventional SI operation to OFC. The movement in the Borghi diagram tends to follow constant-Karlovitz isolines, making it less likely to change into significantly different combustion regimes. Therefore, variations in CR do not pose a risk to the applicability of the *flamelet*-based combustion models discussed above.

Increasing the intake temperature (T_{intake}) raises s_L and decreases l_f [10]. This trend generally follows the opposite path to EGR dilution, moving towards "safer" regions of the Borghi diagram with lower Karlovitz numbers, which are more consistent with the *flamelet* assumption. Consequently, variations in intake temperature do not compromise the validity of the models considered in this study.

Overall, these qualitative trends indicate that while EGR variations require the most careful consideration due to their potential to reach extreme combustion regimes, the control strategies employed in this investigation remain within ranges that preserve the applicability of standard *flamelet*-based models.

3.3. Potential strategies for efficiency improvements

In the previous section, OFC operation was shown to reduce GIE compared with conventional combustion. Thus, this section is devoted to evaluating some strategies to overcome this concept limitation. First, the effect of the EGR ratio will be assessed; later, the influence of the compression ratio will be studied. Finally, the intake temperature will be evaluated to clarify its impact on combustion and engine performance.

Although some of these strategies would require specific adaptation for implementation in a commercial engine, as this is a preliminary fundamental study, the comprehensive development of the required control strategies falls beyond the scope of the work. However, it is

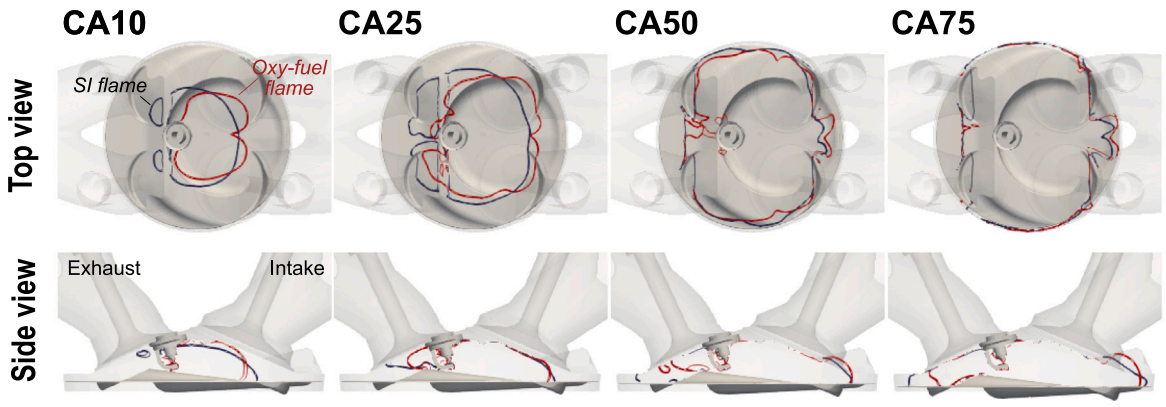

Fig. 10. Flame visualization. The flame front is identified at different combustion timings in both conventional combustion and OFC.

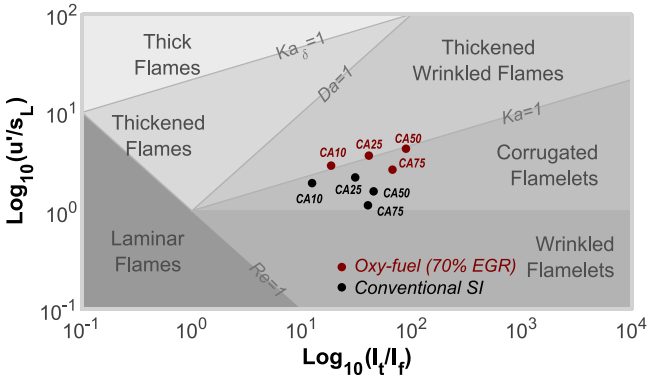

Fig. 11. Combustion regime diagram. The premixed flame regime along the combustion process is shown for conventional and OFC.

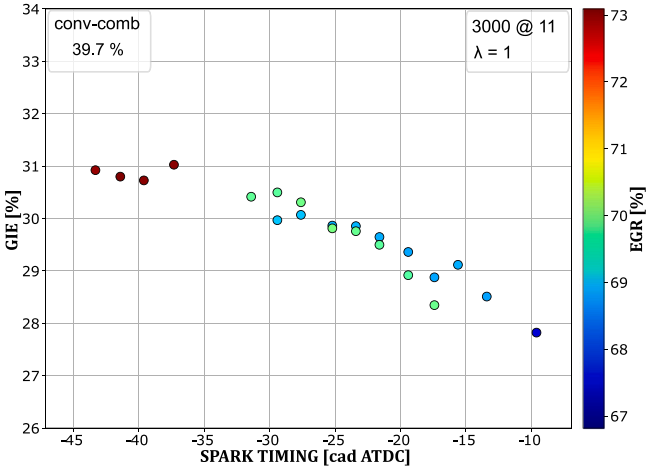

Fig. 12. Experimental OFC GIE as a function of the ST obtained at 3000 rpm, IMEP = 11 bar and $\lambda = 1$.

worth noting that the existing technical solutions can fully cover the requirements. Thus, although knock control in the research engine relies on in-cylinder pressure analysis, implementation in commercial engines would typically be feasible using conventional sensors with minor control calibration adjustments. Similarly, while EGR management requires careful procedures during start-up and stabilization in the single-cylinder engine, established control methodologies from modern engines provide a reliable basis for practical implementation at larger scales. Regarding intake thermal management, intercoolers effectively regulate intake temperature in the controlled test-cell environment; even though real-engine operation may introduce some challenges due to thermal inertia during transient operation, these are not expected to be critical within the intended application range of stationary or large transport systems.

3.3.1. Effects of EGR dilution

Fig. 12 shows the gross indicated efficiency for different EGR ratios and spark advances (ST, from −43 CAD up to −10 CAD, depending on the EGR level) and the reference value under conventional combustion for the sake of comparison (39.7%). On the one hand, the sweep aimed to find the optimal spark and EGR settings for maximum efficiency; on the other hand, the sweep explored the extreme achievable conditions to assess the EGR range previously discussed. As illustrated, when EGR increases from 67% to 73%, the GIE improves by about 4%, reaching a maximum value of 31%. The graph clearly shows that EGR and ST are not independent variables, as the ST range changes with EGR. Thus, at EGR = 68%, the ST range is −30 CAD to −14 CAD, and at EGR = 70%, the ST at which the engine can operate is −32 CAD to −18 CAD. This means that when EGR increases, the ST range is expected to move towards the compression stroke. Additionally, when the ST is delayed (e.g., at ST = −18 CAD), it is better to reduce the dilution ratio, as this will increase the GIE. However, at ST = −30 CAD the opposite strategy should be followed. This behavior can be interpreted from Fig. 13, which shows combustion duration (CA90–CA10) as a function of combustion phasing (CA50) for different EGR levels at $\lambda = 1$. As shown, combustion duration decreases as EGR is reduced because lower dilution enhances mixture reactivity. It also shortens when CA50 is advanced (i.e., at lower ST), since the thermodynamic conditions enhance the combustion process. The combination of both effects shifts the maximum GIE towards higher EGR levels, which requires advancing CA50 to achieve optimal combustion phasing. Therefore, the improvement in GIE is directly associated with the increased dilution provided by higher EGR rates.

Even though the highest GIE is obtained at EGR = 73%, these high dilution operating conditions present a significant cycle-to-cycle variability, and in Fig. 14, this value is quantified with the coefficient of variation of the IMEP ($IMEP_{cov}$). As it is depicted in the graph, for an EGR ratio of 73%, $IMEP_{cov}$ reaches values of 8%, but for a dilution of 70%, $IMEP_{cov}$ values go under 1.5%, which is an admissible value for SI-engines, similar to the value with conventional combustion.

3.3.2. Effect of compression ratio

Given that oxy-fuel combustion tends to diminish in-cylinder pressure, it provides some room for the second potential way to improve the indicated efficiency by increasing the compression ratio. Since the experimental work carried out in previous subsections uses the original engine compression ratio, CR = 11, EGR dilution limits have been

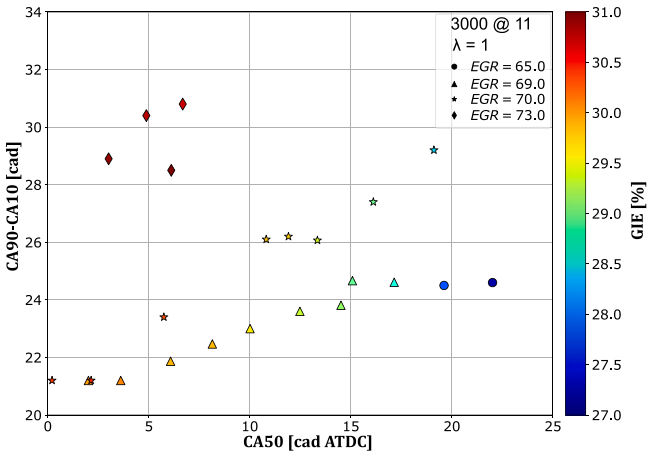

Fig. 13. Experimental OFC CA90-CA10 as a function of the CA50 obtained at 3000 rpm, IMEP = 11 bar and $\lambda = 1$.

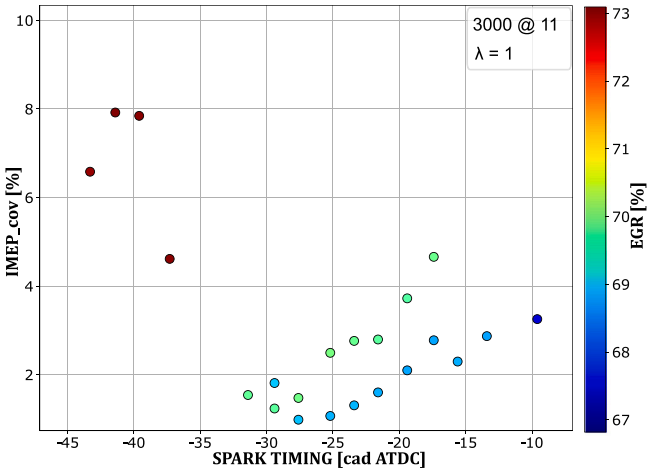

Fig. 14. Experimental $IMEP_{cov}$ obtained at 3000 rpm, IMEP = 11 bar and $\lambda = 1$.

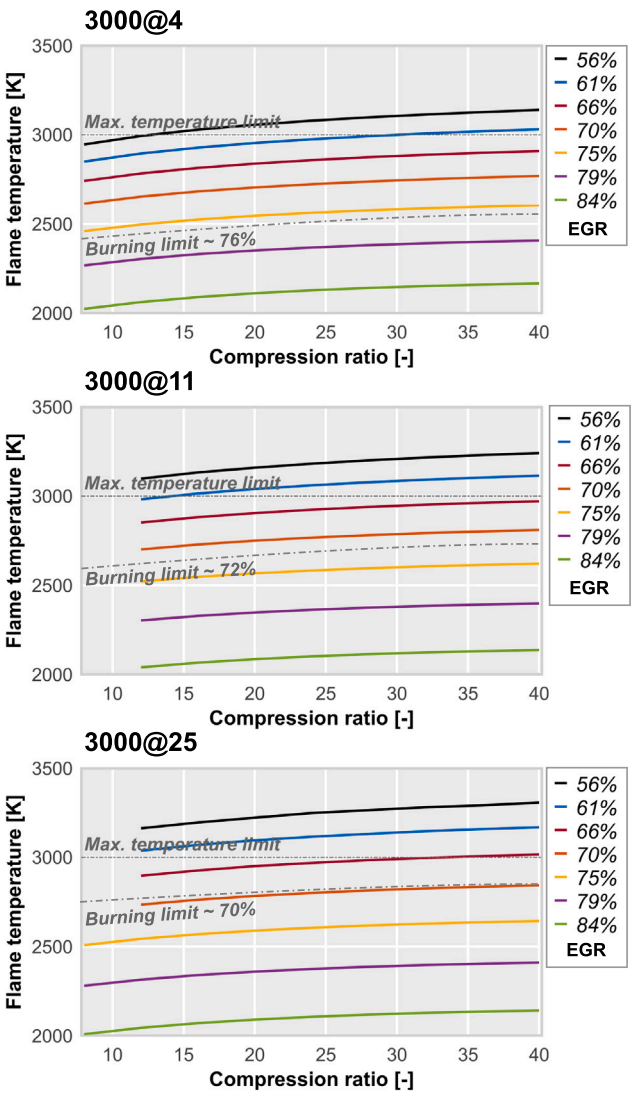

Fig. 15. Effect of the CR and EGR over the flame temperature at $\lambda = 1$.

recalculated as a function of CR using the 0D model, and considering the same thermo-mechanical limitations and the combustion stability threshold already discussed in Section 3.1. Thus, it was possible to assess the potential of increasing the compression ratio to improve efficiency, while accounting for the possibility of knocking. Fig. 15 shows the flame temperature in terms of compression ratio and EGR dilution rate for three loads. In addition, in each graph, the maximum admissible temperature and the burning limit determining the boundary where the combustion can suitably occur at each CR are also plotted.

On the one hand, results show that if CR increases, the minimum EGR rate required to keep the peak in-cylinder temperature below the limit increases to compensate for the effect of the higher temperature of the unburned gases, thus for the 3000@11 case, when CR steps up from 11 to 30, the minimum EGR limit moves from 61% to almost 65% respectively. On the other hand, the maximum EGR rate appears to be stable with CR; this is due to the combined effect of higher temperature and pressure: the former enhances the laminar combustion velocity, while the latter slows it down. These global trends are similar in the three loads modeled.

Regarding the effect of the load, it can be stated that, on the one hand, the burning limit causes the maximum EGR value to decrease from 76% to 70% as the load increases from 4 bar to 25 bar, due to the effect of pressure on combustion velocity. On the other hand, the minimum EGR increases with the load to avoid exceeding the maximum temperature.

As a combination of the trends with CR and load, it can be seen that the operation range, in EGR terms, becomes smaller when the load increases, thus at 3000@4 and CR = 11 the engine can operate in the EGR range of [56% to 76%], while at 3000@25 and CR = 30 the range is reduced to [66% to 70%]; thus, being necessary a more accurate control for this variable to ensure the safe and stable operation.

Once the dilution analysis was performed, the maximum CR that could be used to recover the GIE drop was set by conducting a knocking analysis under the high-load condition, where this phenomenon is more likely to occur. To this end, the effect of the CR on the heat release rate and in-cylinder pressure has been calculated with the 1D-CFD approach for the 3000@25 operating condition, with an $EGR = 70\%$ and a constant spark timing (ST) of −20 CAD. This EGR level was selected because it almost coincides with the highest EGR level for stable combustion in all the CR plotted in Fig. 15 at 3000@25. Results are shown in Fig. 17, and they indicate that the maximum in-cylinder pressure grows gradually up to 10 MPa when the CR increases from 11 to 22, but beyond that value, the maximum pressure significantly rises, reaching values of 17 MPa and 32 MPa when the CR shifts to 24 and 28, respectively. Moreover, up to CR = 22, the maximum HRR values are below 80 J/CAD, but at higher CR values, combustion becomes abrupt,

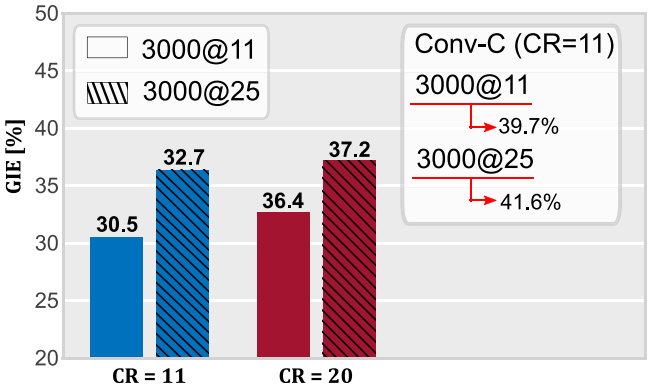

Fig. 16. Effect of the CR over the GIE for 3000@11 and 3000@25 at $\lambda = 1$.

with HRR peaks exceeding 200 J/CAD. Accordingly, based on these results, it can be concluded that a high knocking propensity can be expected with OFC if CR is greater than 20 with EGR=70%. The same analysis was repeated using the 1D-CFD coupling method for different EGR rates to determine the limit at which this phenomenon is likely to appear; it is included in Fig. 18 along with the other restrictions already discussed. Therefore, while the EGR decreases from 70% to 66% the CR could increase from 24 to 27. This effect can be explained by the fact that the higher combustion velocity, due to the lower dilution, counteracts the higher reactivity of the end gas. Taking into account all the restrictions, in Fig. 16 the GIE is depicted as a function of the CR. It is worth noting that the GIE values at 3000@11 and CR = 11 for the conventional and OFC cases were experimentally obtained, whereas the high load results were predicted using the 1D-CFD coupling method. At the middle load, it is predicted that a performance improvement of around 5.9 pp will occur when the CR switches from 11 to 20. This improvement set the GIE for the OFC case to 36.4% (about 3.3 pp below the conventional combustion case). When this strategy is evaluated at high load, the OFC efficiency increases by 4.5 pp. Thus, at CR = 20, the GIE is expected to reach approximately 37.2%, which is still about 4 pp below the conventional combustion case. To summarize, at the original engine compression rate (CR = 11), the GIE in the OFC case was around 9 pp lower than in conventional combustion. Since knocking is less likely to occur in OFC mode, the compression ratio can be increased to CR = 20. Thus, the efficiency gap between the two combustion modes was reduced to only 3-4 pp.

3.3.3. Effect of intake temperature

Up to this point, results show that as load increases, the maximum achievable EGR ratio required to maintain combustion stability decreases (for a given CR); thus, it limits the EGR potential to improve the GIE, as discussed in Section 3.3.1. To complete the assessment of the parameters affecting the indicated efficiency, this subsection analyzes the effect of intake temperature. Gas temperature directly affects the combustion process, thereby influencing combustion duration and stability, and can provide additional room to further increase EGR dilution. Thus, final performance and knocking will result from the combined effects of temperature and EGR.

In the previous analysis, all the experimental measurements described in Section 3.2 and the later simulations carried out in Sections 3.3.1 and 3.3.2, have been performed with an intake temperature of 80 °C (353 K). It was experimentally checked that, with EGR rates around 70%, the high water vapor concentration at the intake leads to condense part of the water if the intake temperature is lower to 80 °C; thus, at 70 °C (343 K), it is estimated that 1.5 l/h of liquid water condensed in the intake line (downstream of the EGR and oxygen mixture plenum). At 60 °C (333 K), about 1.5 l/h is condensed during EGR conditioning, and an additional 0.5 l/h in the intake line, which

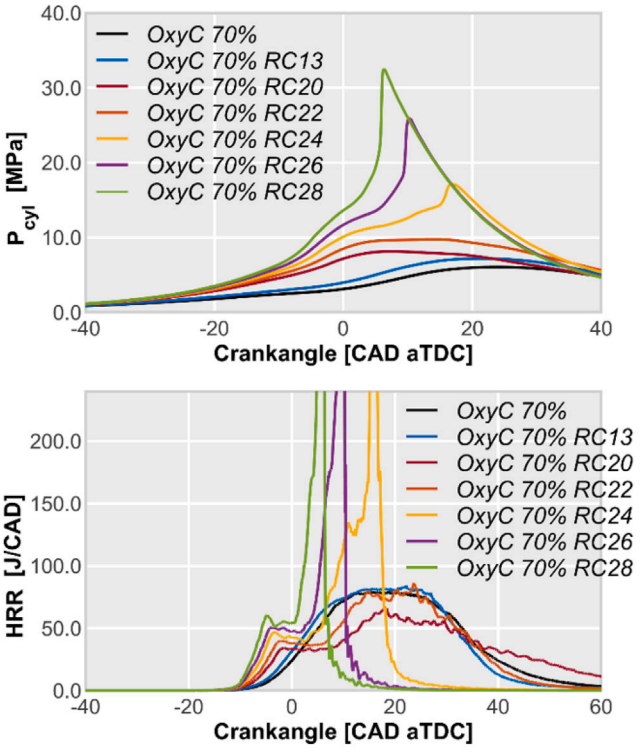

Fig. 17. Effect of the CR over the in-cylinder and the RoHR at 3000@25, $\lambda = 1$ and EGR=70%.

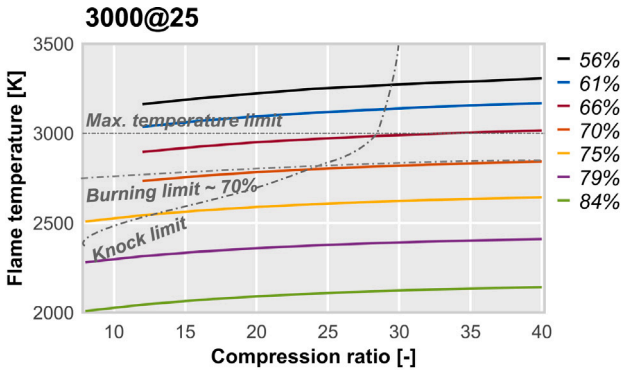

Fig. 18. Effect of the CR and EGR over the flame temperature for 3000@25 and $\lambda = 1$ with knock limitation.

then enters the engine as liquid drops. Even though the thermodynamic conditions in the chamber ensure that most of this liquid is later re-evaporated during compression, some of it is deposited on the chamber walls during the intake and initial compression periods. Hence, with a lower intake temperature than 80 °C there is a slight risk of oil contamination with liquid water. Moreover, if part of the water is condensed at the intake, gas analysis becomes more difficult and uncertain, as mass balances are affected. These phenomena led to avoiding evaluating intake temperatures below 80 °C; thus, the following theoretical evaluation of the temperature impact was carried out by increasing this variable.

Fig. 19 shows, for the 3000@25 operating condition, the influence that intake temperature has on the flame temperature, the laminar flame speed, and the auto-ignition delay as a function of the EGR. These results were calculated with the 0D-1D thermochemical model, as done in Section 3.1. As the intake temperature increases from 350 K to 465 K, the minimum EGR required to avoid exceeding the maximum

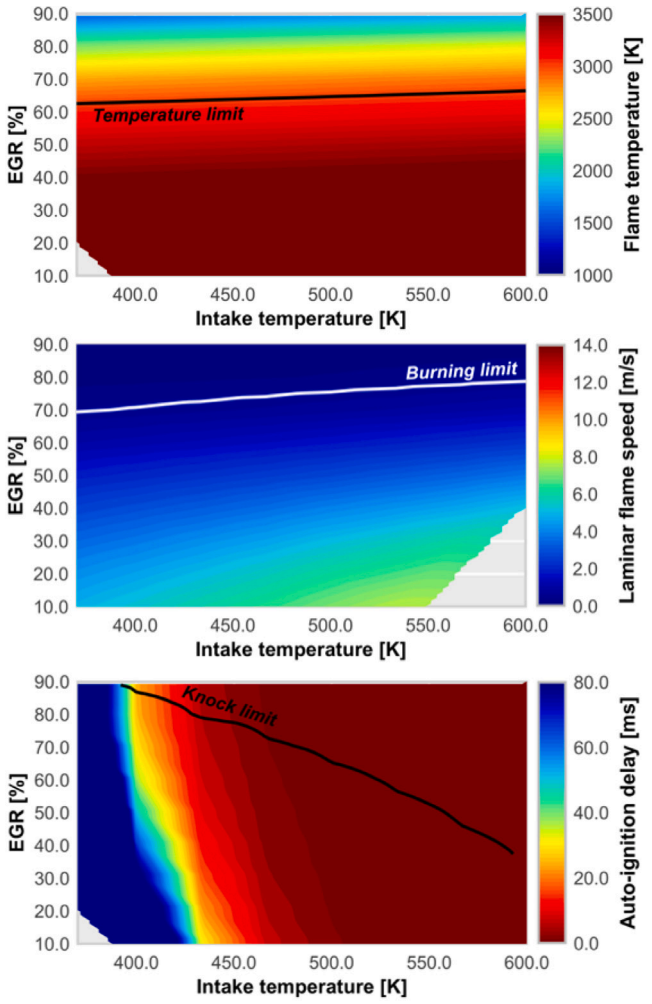

Fig. 19. Effect of the intake temperature over the combustion parameters at 3000@25 and $\lambda = 1$.

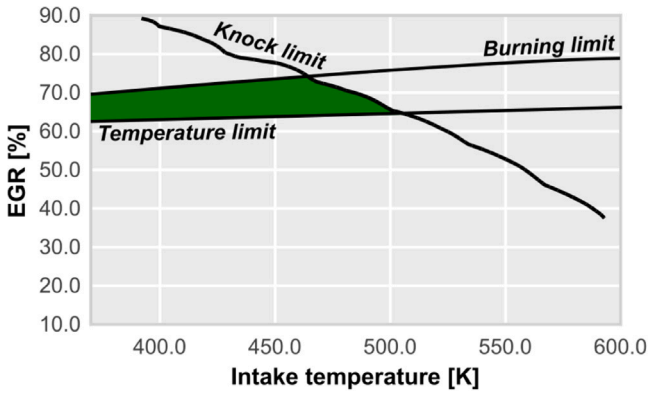

Fig. 20. OFC operating region as a function of intake temperature at 3000@25 and $\lambda = 1$.

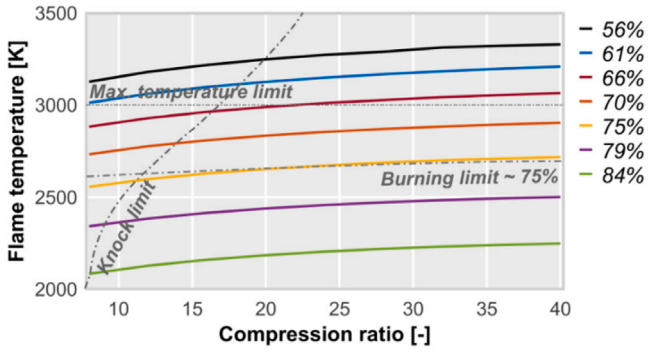

Fig. 21. Effect of the CR and EGR ratio over the flame temperature at 3000@25, $\lambda = 1$ and $T_{intake} = 465$ K.

in-cylinder temperature (3000 K) shifts from 62% to 64%. At the same time, the maximum EGR limited by the burning velocity increases from 70% to 75%. Although increasing the temperature allows achieving higher EGR dilution, the reduction in auto-ignition delay increases knocking propensity; thus, if the intake temperature exceeds 465 K, the maximum EGR should be reduced from 75% to 65% to avoid knocking. To summarize, the three aforementioned restrictions are shown in Fig. 20, highlighting in green the region where the engine can operate with stable combustion and safe conditions under OFC at the original engine compression ratio (CR = 11).

To evaluate the combination of increasing the intake temperature in combination with higher CR, Fig. 21 shows the flame temperature for a constant intake temperature of 465 K (a conservative value derived from Fig. 20) the maximum CR that could be used to avoid knocking. The procedure used is based on the 1D-CFD approach, as described in Section 3.3.2. Results reveal that for an EGR ratio of 70% the maximum CR will be about 14; meanwhile, for an intake temperature of 350 K, the limit is set up to 22 (see Fig. 18). However, it is possible to reach an EGR ratio of 75% at 465 K, but in this case, the maximum CR is 12.

Considering the aforementioned effects of intake temperature, the next step was to predict the impact of this temperature change on performance. This was achieved using the 1D-CFD modeling, with which the GIE was calculated for the oxy-fuel combustion internal combustion engine operating at an intake temperature of 465 K and an EGR ratio of 75% at 3000@25. Even though the CR could be increased to 12, it was decided to maintain the original value (CR = 11) to ensure a safety margin and assess the change in operating condition without modifying any geometrical parameters. Results showed that when the operating point is switched from 80 °C and EGR = 70%, to 192 °C (465 K) and EGR = 75%, the GIE will increase 1.5 pp. This means that the GIE could increase from 32.7% to 34.2%.

4. Conclusions

The work provides a comprehensive assessment of premixed oxy-fuel combustion (OFC) in SI engines, elucidating the role of humid EGR and O_2 dilution and exploring improvement strategies through combined experimental and 0D–1D/CFD numerical analyses. The main findings are:

- Simulations allowed assessing the operating limits and performance trends of premixed OFC beyond the conditions tested. Results show that OFC enables engine operation over a wide dilution range, including O_2 excess and EGR. Considering combustion stability, thermal limits, and knock propensity, a feasible domain was identified, ranging from $\lambda = 1$ operation with 61%–73% EGR to lean conditions up to $\lambda = 4$ with approximately 35% EGR. From a technological perspective, EGR-based dilution at $\lambda = 1$ was identified as the most suitable option. Under these conditions, the low knock tendency allows an increase in compression ratio from 11 to 20, improving the gross indicated efficiency (GIE) by about 5 percentage points. Numerical results also indicate that intake temperature is an effective control parameter to extend the EGR range and recover GIE, but its benefits are coupled with knock limitations, requiring a careful trade-off with EGR and compression ratio.

- From an experimental standpoint, stable premixed OFC operation was demonstrated at $\lambda = 1$ with EGR rates of approximately 67%–73%, in good agreement with the simulated range predicted (the lower limit was experimentally constrained by the exhaust temperature specifications of the engine). Under these conditions, NO_x emissions were reduced by more than 99% relative to conventional air combustion, while CO and uHC were reduced by up to 89%. Experimental results also showed a reduction of up to 9 percentage points in GIE compared to conventional combustion, mainly due to slower combustion and the lower specific heat ratio of the mixture.
- The main drawback of OFC is the aforementioned gross indicated efficiency reduction, which can reach up to 9 percentage points. However, there is room for efficiency improvement through design-oriented strategies, such as increasing the compression ratio to enable approximately 5 percentage points of recovery and reducing the final efficiency penalty to about 3%–4%.
- OFC-ICE can be regarded as a promising transitional solution for decarbonization, combining the maturity of ICE technology with CO_2 capture. However, further work is required to fully evaluate its viability. Experimental validation should be extended to a wider operating range, including higher loads and multi-cylinder configurations, and the combined effects of compression ratio, dilution strategy, and intake temperature should be assessed experimentally.

List of acronyms

AID	Auto-ignition delay
AMR	Adaptive Mesh Refinement
BSFC	Brake Specific Fuel Consumption
CAD	Crank Angle Degree
CFD	Computational Fluid Dynamics
CO	Carbon Monoxide
CR	Compression Ratio
EGR	Exhaust Gas Recirculation
EVO	Exhaust Valve Opening
GIE	Gross Indicated Efficiency
HC	Hydrocarbons
HR	Heat Release
HRR	Heat Release Rate
ICE	Internal Combustion Engine
IMEP	Indicated Mean Effective Pressure
IVC	Intake Valve Closing
MIEC	Mixed Ionic and Electronic Conducting
MZ	Multi-Zone
NO_x	Nitric Oxides
OFC	Oxy-Fuel Combustion
OTM	Oxygen Transport Membrane
PFI	Port Fuel Injection
PID	Proportional-Integral-Derivative
PISO	Pressure Implicit with Splitting of Operators
PRF	Primary Reference Fuel
SI	Spark Ignition
ST	Spark Timing
TDC	Top Dead Center
uHC	Unburned Hydrocarbons
URANS	Unsteady Reynolds-Averaged Navier–Stokes

CRediT authorship contribution statement

R. Raggi: Writing – original draft, Visualization, Validation, Methodology, Investigation, Data curation. **J. Gomez-Soriano:** Writing – review & editing, Software, Investigation, Conceptualization. **J. Martín:** Writing – review & editing, Supervision, Project administration, Investigation, Conceptualization. **R. Novella:** Supervision, Project administration, Funding acquisition.

Declaration of competing interest

The authors declare that they have no known competing financial interests or personal relationships that could have appeared to influence the work reported in this paper.

Acknowledgments

This work has been partially supported by Grant PID2021-123351OB-I00 funded by MCIN/AEI/ 10.13039/501100011033, Spain and, as appropriate, by "ERDF A way of making Europe", and by Generalitat Valenciana, Spain through the grant Santiago Grisolía GRISOLIAP/2021/108. The authors want to express their gratitude to CONVERGENT SCIENCE Inc. and Convergent Science GmbH for their kind support with the CFD calculations using the CONVERGE software.

Funding for open access charge: CRUE-Universitat Politécnica de Valéncia.

The authors would like to thank Ing. Gabriel Alcantarilla Ballesteros for his inestimable work during the experimental campaign.

Data availability

Data will be made available on request.

References

[1] European Commission. COM(2014) 15 final: A policy framework for climate and energy in the period from 2020 to 2030. 2014.
[2] European Commission. Determining the environmental impacts of conventional and alternatively fuelled vehicles through LCA. 2020.
[3] Maiello A, Novella R, Gomez-Soriano J, Beatrice C. Evaluation of CNG engine conversion to hydrogen fuel for stationary and transient operations. Energy Convers Manage 2025;326:119425.
[4] Molina S, Gómez-Soriano J, Lopez-Juarez M, Olcina-Girona M. Evaluation of the environmental impact of HCNG light-duty vehicles in the 2020–2050 transition towards the hydrogen economy. Energy Convers Manage 2024;301:117968.
[5] European Environment Agency. National emissions reported to the convention on long-range transboundary air pollution (LRTAP convention). 2021.
[6] Tan Q, Hu Y. A study on the combustion and emission performance of diesel engines under different proportions of O2 & N2 & CO2. Appl Therm Eng 2016;108:508–15.
[7] Serrano JR, Bracho G, Gomez-Soriano J, Fernandes C. Development of an oxy-fuel combustion system in a compression-ignition engine for ultra-low emissions powerplants using CFD and evolutionary algorithms. Appl Sci 2022;12(14):7104.
[8] Escudero AI, Espatolero S, Romeo LM. Oxy-combustion power plant integration in an oil refinery to reduce CO2 emissions. Int J Greenh Gas Control 2016;45:118–29.
[9] Serrano JR, Piqueras P, Sanchis EJ, García FJ. Comparative life cycle assessment of oxy-fuel combustion utilization across various fuels in the maritime sector. Energy Convers Manage 2025;342:120034.
[10] Serrano JR, Díaz JM, Gomez-Soriano J, Raggi R. Exploring the oxy-fuel combustion in spark-ignition engines for future clean powerplants. J Eng Gas Turbines Power 2023;145(10):101006.
[11] Pei X, He B, Yan L, Wang C, Song W, Song J. Process simulation of oxy-fuel combustion for a 300 MW pulverized coal-fired power plant using aspen plus. Energy Convers Manage 2013;76:581–7.
[12] Serrano J, Martín J, Gomez-Soriano J, Raggi R. Theoretical and experimental evaluation of the spark-ignition premixed oxy-fuel combustion concept for future CO2 captive powerplants. Energy Convers Manage 2021;244:114498.
[13] Wu Z, Yu X, zhong Fu L, Deng J, guang Li L. Experimental study of the effect of water injection on the cycle performance of an internal-combustion Rankine cycle engine. Proc Inst Mech Eng Part D: J Automob Eng 2014;228(5):580–8.
[14] Li X, Pei Y, Li D, Ajmal T, Rana K-J, Aitouche A, Mobasheri R, Peng Z. Effects of water injection strategies on oxy-fuel combustion characteristics of a dual-injection spark ignition engine. Energies 2021;14(17).
[15] Serrano JR, Arnau FJ, García-Cuevas LM, Farias VH. Oxy-fuel combustion feasibility of compression ignition engines using oxygen separation membranes for enabling carbon dioxide capture. Energy Convers Manage 2021;247:114732.

[16] Baumann S, Serra J, Lobera M, Escolástico S, Schulze-Küppers F, Meulenberg W. Ultrahigh oxygen permeation flux through supported Ba0.5Sr0.5Co0.8Fe0.2O3-δ membranes. J Membr Sci 2011;377(1–2):198–205.
[17] Catalán-Martínez D, Santafé-Moros A, Gozálvez-Zafrilla JM, García-Fayos J, Serra J. Characterization of oxygen transport phenomena on BSCF membranes assisted by fluid dynamic simulations including surface exchange. Chem Eng J 2020;387:124069.
[18] Benajes J, Olmeda P, Martín J, Carreño R. A new methodology for uncertainties characterization in combustion diagnosis and thermodynamic modelling. Appl Therm Eng 2014;71(1):389–99.
[19] Bounaceur R, Glaude P-A, Sirjean B, Fournet R, Montagne P, Vierling M, Moliere M. Prediction of auto-ignition temperatures and delays for gas turbine applications. J Eng Gas Turbines Power 2016;138:021505.
[20] Liu Y-D, Jia M, Xie M-Z, Pang B. Enhancement on a skeletal kinetic model for primary reference fuel oxidation by using a semidecoupling methodology. Energy & Fuels 2012;26(12):7069–83.
[21] Benajes J, Novella R, Gomez-Soriano J, Barbery I, Libert C, Rampanarivo F, Dabiri M. Computational assessment towards understanding the energy conversion and combustion process of lean mixtures in passive pre-chamber ignited engines. Appl Therm Eng 2020;178:115501.
[22] Fieweger K, Blumenthal R, Adomeit G. Self-ignition of SI engine model fuels: a shock tube investigation at high pressure. Combust Flame 1997;109(4):599–619.
[23] Gülder ÖL. Correlations of laminar combustion data for alternative SI engine fuels. Tech. rep., SAE Technical Paper; 1984.
[24] Jerzembeck S, Peters N, Pepiot-Desjardins P, Pitsch H. Laminar burning velocities at high pressure for primary reference fuels and gasoline: Experimental and numerical investigation. Combust Flame 2009;156(2):292–301.
[25] Heimel S, Weast RC. Effect of initial mixture temperature on the burning velocity of benzene-air, n-heptane-air, and isooctane-air mixtures. In: Symposium (international) on combustion. Vol. 6, (1):Elsevier; 1957, p. 296–302.
[26] Sforza L, Ramognino F, Cerri T, Gianetti GG, D'Errico G, Onorati A, Gomez-Soriano J, Novella R. A 1D-3D numerical study of a pent-roof spark-ignition engine fueled with hydrogen lean mixtures. Int J Engine Res 2025.
[27] CONVERGE 2.4 theory manual. 2018.
[28] Yakhot V, Orszag SA. Renormalization group analysis of turbulence. I. Basic theory. J Sci Comput 1986;1(1):3–51.
[29] Angelberger C, Poinsot T, Delhay B. Improving near-wall combustion and wall heat transfer modeling in SI engine computations. Tech. rep., SAE Technical Paper; 1997.
[30] Torregrosa AJ, Broatch A, Margot X, Gomez-Soriano J. Understanding the unsteady pressure field inside combustion chambers of compression-ignited engines using a computational fluid dynamics approach. Int J Engine Res 2020;21(8):1273–85.
[31] Issa RI. Solution of the implicitly discretised fluid flow equations by operator-splitting. J Comput Phys 1986;62(1):40–65.
[32] Senecal P, Pomraning E, Richards K, Briggs T, Choi C, McDavid R, Patterson M. Multi-dimensional modeling of direct-injection diesel spray liquid length and flame lift-off length using CFD and parallel detailed chemistry. SAE Trans 2003;1331–51.
[33] Babajimopoulos A, Assanis D, Flowers D, Aceves S, Hessel R. A fully coupled computational fluid dynamics and multi-zone model with detailed chemical kinetics for the simulation of premixed charge compression ignition engines. Int J Engine Res 2005;6(5):497–512.
[34] Scarcelli R, Matthias N, Wallner T. Numerical investigation of combustion in a lean burn gasoline engine. SAE Tech Pap 2013.
[35] Pal P, Probst D, Pei Y, Zhang Y, Traver M, Cleary D, Som S. Numerical investigation of a gasoline-like fuel in a heavy-duty compression ignition engine using global sensitivity analysis. SAE Int J Fuels Lubr 2017;10(1):56–68.
[36] Yang X, Solomon A, Kuo T-W. Ignition and combustion simulations of spray-guided SIDI engine using arrhenius combustion with spark-energy deposition model. SAE Tech Pap 2012.
[37] Torregrosa A, Olmeda P, Degraeuwe B, Reyes M. A concise wall temperature model for DI diesel engines. Appl Therm Eng 2006;26(11–12):1320–7.
[38] Luján J, Arnau F, Piqueras P, Farias V. Design of a carbon capture system for oxy-fuel combustion in compression ignition engines with exhaust water recirculation. Energy Convers Manage 2023;284.
[39] Arnau FJ, Benajes JV, Catalán D, Desantes JM, García-Cuevas LM, Serra JM, Serrano JR. Internal combustion engine and operating method of the same. Motor de combustión interna y método de funcionamiento del mismo, P201930285, 28.03.2019. WO2020/193833A1, 01.10.2020. PCT/ES2020/070199, 21.03.2020. ES2751129B2, 29.03.2021.
[40] Payri F, Olmeda P, Martin J, Carreño R. A new tool to perform global energy balances in DI diesel engines. SAE Int J Engines 2014;7(1):43–59.
[41] Benajes J, Novella R, Gomez-Soriano J, Martinez-Hernandiz P, Libert C, Dabiri M. Evaluation of the passive pre-chamber ignition concept for future high compression ratio turbocharged spark-ignition engines. Appl Energy 2019;248:576–88.
[42] Peters N. Turbulent combustion. 2001.